PHYSICAL REVIEW D **80,** 083505 (2009)

Cluster constraints on $f(R)$ gravity

Fabian Schmidt,[1] Alexey Vikhlinin,[2] and Wayne Hu[1]

[1]*Kavli Institute for Cosmological Physics, Department of Astronomy & Astrophysics, and Enrico Fermi Institute, University of Chicago, Chicago, Illinois 60637, USA*

[2]*Harvard-Smithsonian Center for Astrophysics, 60 Garden Street, Cambridge, Massachusetts 02138, USA, and Space Research Institute, Moscow, Russia*

(Received 17 August 2009; published 6 October 2009)

Modified gravitational forces in models that seek to explain cosmic acceleration without dark energy typically predict deviations in the abundance of massive dark matter halos. We conduct the first, simulation calibrated, cluster abundance constraints on a modified gravity model, specifically the modified action $f(R)$ model. The local cluster abundance, when combined with geometric and high redshift data from the cosmic microwave background, supernovae, H_0, and baryon acoustic oscillations, improves previous constraints by nearly 4 orders of magnitude in the field amplitude. These limits correspond to a 2 order of magnitude improvement in the bounds on the range of the force modification from the several Gpc scale to the tens of Mpc scale.

DOI: 10.1103/PhysRevD.80.083505 PACS numbers: 98.80.−k, 04.50.Kd, 95.36.+x

I. INTRODUCTION

In $f(R)$ models, cosmic acceleration arises not from an exotic form of energy with negative pressure but from a modification of gravity. Here the Einstein-Hilbert action is augmented by a general function $f(R)$ of the Ricci or curvature scalar R [1–3]. Such modifications not only can accelerate the background expansion but also generically lead to enhancements in gravitational forces on small scales.

$f(R)$ gravity is equivalent to a scalar-tensor theory, where $f_R = df/dR$ is the additional scalar degree of freedom. This field has a mass and propagates on scales smaller than the associated Compton wavelength. Well within the Compton wavelength, the scalar mediates a $4/3$ enhancement of gravitational forces, with corresponding strong effects on the growth of structure in the Universe. These enhancements are quantified by the mass of the field or equivalently by the value of the field in the background, f_{R0}. In order to pass stringent Solar System constraints, viable $f(R)$ models employ the chameleon effect which allows the field to become very massive in high-density environments [4]. However, in order for the chameleon effect to become active, the background field should be smaller than the typical depth of cosmological potential wells, $|f_{R0}| < |\Psi| \sim 10^{-6}$–$10^{-5}$ [5].

Independently of this Solar System constraint, however, it is worth studying the constraints that can be placed on $f(R)$ gravity directly from cosmological observations. In the linear regime, these provide only weak constraints. Changes in the low multipole anisotropy of the cosmic microwave background (CMB) only place order unity bounds on the value of f_{R0}, while changes to the shape of the matter power spectrum, though larger, can be mimicked by galaxy bias [6].

The effect of enhanced forces can be substantially more prominent in the nonlinear regime. Cosmological simulations have shown that for field values larger than $|f_{R0}| \sim 10^{-5}$ the abundances of rare massive halos are enhanced substantially [7]. Counts of galaxy clusters therefore provide the opportunity to improve cosmological constraints on $f(R)$ models ultimately by 4–5 orders of magnitude.

In this paper, we quantify current cluster abundance constraints on $f(R)$ models from a combined sample of low-redshift x-ray clusters. We begin in Sec. II A with a description of the model and its impact on cluster predictions. In Sec. III we describe the likelihood analysis of the local cluster abundance data. We combine these constraints with geometric and high redshift constraints in Sec. IV to obtain upper limits on the modification to gravity. We discuss these results in Sec. V.

II. $f(R)$ CLUSTER ABUNDANCE

In this section, we describe the enhancement that $f(R)$ models make to the cluster abundance. We begin in Sec. II A with a brief review of the $f(R)$ model itself. We describe cosmological simulations with representative parameter choices in Sec. II B which are used to calibrate mass function enhancements across a wider range of parameters in Sec. II C.

A. $f(R)$ model

In the $f(R)$ model, the Einstein-Hilbert action is augmented with a general function of the scalar curvature R,

$$S_G = \int d^4x\sqrt{-g}\left[\frac{R + f(R)}{16\pi G}\right]. \tag{1}$$

Here and throughout $c = \hbar = 1$. Gravitational force enhancements are associated with an additional scalar degree of freedom $f_R \equiv df/dR$ and have a range given by the Compton wavelength $\lambda_C = (3df_R/dR)^{1/2}$. This additional

 © 2009 The American Physical Society

attractive force leads to the enhancement in the abundance of rare massive dark matter halos described below.

For definiteness, we choose the functional form for $f(R)$ given in [5] (with $n = 1$):

$$f(R) = -2\Lambda \frac{R}{R + \mu^2}, \tag{2}$$

with two free parameters, Λ and μ^2. Note that as $R \to 0$, $f(R) \to 0$, and hence the model does not contain a cosmological constant. For $R \gg \mu^2$, the function $f(R)$ can be approximated as

$$f(R) = -2\Lambda - f_{R0} \frac{\bar{R}_0^2}{R}, \tag{3}$$

with $f_{R0} = -2\Lambda\mu^2/\bar{R}_0^2$ replacing μ as the second parameter of the model. Here we define $\bar{R}_0 = \bar{R}(z = 0)$, so that $f_{R0} = f_R(\bar{R}_0)$, where overbars denote the quantities of the background spacetime. Note that if $|f_{R0}| \ll 1$ the curvature scales set by $\Lambda = \mathcal{O}(R_0)$ and μ^2 differ widely and hence the $R \gg \mu^2$ approximation is valid today and for all times in the past.

The background expansion history mimics ΛCDM with Λ as a true cosmological constant to order f_{R0}. Therefore in the limit $|f_{R0}| \ll 10^{-2}$, the $f(R)$ model and ΛCDM are essentially indistinguishable with geometric tests. Nonetheless geometric tests do constrain one of the two parameters (Λ) leaving the cluster abundance to constrain the other parameter (f_{R0}) which controls the strength and range of the force modification. With the functional form of Eq. (3), the comoving Compton wavelength becomes

$$\frac{\lambda_C}{1 + z} = \sqrt{6|f_{R0}| \frac{R_0^2}{R^3}}, \tag{4}$$

with a value today of

$$\lambda_{C0} \approx 32 \sqrt{\frac{|f_{R0}|}{10^{-4}}}\ \text{Mpc}. \tag{5}$$

The behavior of $f(R)$ gravity is described by the modified Einstein equations. Specifically, the trace of the linearized Einstein equations yields the f_R field equation

$$\nabla^2 \delta f_R = \frac{a^2}{3}[\delta R(f_R) - 8\pi G \delta\rho_m], \tag{6}$$

where time derivatives have been neglected compared with spatial derivatives, coordinates are comoving, $\delta f_R = f_R(R) - f_R(\bar{R})$, $\delta R = R - \bar{R}$, and $\delta\rho_m = \rho_m - \bar{\rho}_m$. Note that the local curvature R is given as a function of the local field value f_R. The time-time component returns the modified Poisson equation

$$\nabla^2 \Psi = 4\pi G a^2 \delta\rho_m - \tfrac{1}{2}\nabla^2 \delta f_R. \tag{7}$$

Here Ψ is the Newtonian potential or time-time metric perturbation $2\Psi = \delta g_{00}/g_{00}$ in the longitudinal gauge. These two equations define a closed system for the Newtonian potential given the density field. The matter falls in the Newtonian potential as usual and so the modifications to gravity are completely contained in the equation for Ψ.

Because of the conformal equivalence of $f(R)$ and scalar-tensor theories and the conformal invariance of electromagnetism, the geodesics of photons are unmodified by the presence of the scalar f_R field save for conformal rescaling factors of $1 + f_R$ [8]. This means that given a fixed density field, e.g. a halo of mass M, the *lensing* potential will be identical to the one in general relativity (GR) in the $|f_R| \ll 1$ limit that we work in. In other words, we will measure the ''true'' mass M through lensing.

On the other hand, the mass inferred from dynamical measures, $M_{\rm dyn}$, such as velocities and virial temperatures is related to the *dynamical* potential which will be different in the presence of the f_R field. In the low curvature limit where $\delta R \ll 8\pi G \delta\rho_m$, Eq. (7) shows that the dynamical potential will be enhanced by $4/3$. Hence the mismatch between $M_{\rm dyn}$ and M could be as large as 33%. Conversely, field fluctuations can saturate in deep gravitational potentials as $f_R \to 0$. Here $\delta R \approx 8\pi G \delta\rho_m$ and force modifications disappear via the chameleon mechanism. Then, if the whole mass is contained in the saturated region, $M_{\rm dyn} = M$. We discuss the mass calibration of the cluster sample in Sec. III.

B. Simulations

We use a modified N-body simulation as described in [9] and used in [7,10] to quantify the impact of the force modification on the cluster abundance. Specifically we employ the system of equations defined by the modified Poisson equation (7) and the f_R field equation (6) in the context of cosmological structure formation. The field equation for f_R is solved on a fixed cubic grid, using a nonlinear relaxation algorithm. The potential Ψ is computed from the density and f_R fields using the fast Fourier transform method. The dark matter particles are then moved according to the gradient of the computed potential, $-\nabla\Psi$.

The simulations were performed for a range of background field values $|f_{R0}| = 10^{-6}$–10^{-4}. We also simulated $|f_{R0}| = 0$ which is equivalent to ΛCDM, using the same initial conditions. Note that the background expansion history for all runs is indistinguishable from ΛCDM to $\mathcal{O}(f_{R0})$.

Cosmological parameters were fixed in the simulations to a flat $\Omega_\Lambda = 0.76$, $\Omega_b = 0.04181$, $H_0 = 73$ km/s/Mpc model and initial power in curvature fluctuations $A_s = (4.82 \times 10^{-5})^2$ at $k = 0.02\ \text{Mpc}^{-1}$ with a tilt of $n_s = 0.958$. All simulations possess 512 grid cells in each direction and $N_p = 256^3$ particles. Halos were identified in the simulations using a standard spherical overdensity halo finder [7]. In the next section, we describe our model for the $f(R)$ effects on the halo mass function, which allows us

to extend predictions to a range of cosmological parameter values.

C. Mass function enhancement

In order to properly marginalize constraints over cosmological parameters, we need a prediction of the mass function enhancement as a function of cosmological parameters and the $f(R)$ parameter f_{R0}. Because of the large computing requirements for full $f(R)$ simulations [9], running simulations for a range of parameters are not feasible, and we use a model of the mass function enhancement based on spherical collapse and the Sheth-Tormen (ST) prescription (see [7] for details). Note that we use this prescription and the cosmological simulations that calibrate it to compute enhancements only. For the ΛCDM baseline predictions, we use mass function results from state-of-the-art numerical simulations (see Sec. III A).

The ST description for the comoving number density of halos per logarithmic interval in the virial mass M_v is given by

$$n_{\ln M_v} \equiv \frac{dn}{d\ln M_v} = \frac{\bar{\rho}_m}{M_v} f(\nu) \frac{d\nu}{d\ln M_v}, \tag{8}$$

where the peak threshold $\nu = \delta_c/\sigma(M_v)$ and

$$\nu f(\nu) = A\sqrt{\frac{2}{\pi} a\nu^2}[1 + (a\nu^2)^{-p}]\exp[-a\nu^2/2]. \tag{9}$$

Here $\sigma(M)$ is the variance of the linear density field convolved with a top hat of radius r that encloses $M = 4\pi r^3 \bar{\rho}_m/3$ at the background density

$$\sigma^2(r) = \int \frac{d^3k}{(2\pi)^3} |\tilde{W}(kr)|^2 P_L(k), \tag{10}$$

where $P_L(k)$ is the linear power spectrum and $\tilde{W}$ is the Fourier transform of the top hat window. The normalization constant A is chosen such that $\int d\nu f(\nu) = 1$. The parameter values of $p = 0.3$, $a = 0.75$, and $\delta_c = 1.673$ for the spherical collapse threshold have previously been shown to match simulations of ΛCDM at the 10%–20% level. The virial mass is defined as the mass enclosed at the virial radius r_v, at which the average density is Δ_v times the critical density $\rho_{\rm cr}$. For consistency with cluster analyses, overdensities will refer to critical density throughout the paper; the corresponding overdensities in terms of the background matter density are given by $\Delta_{\rho_m} = \Delta_{\rho_{\rm cr}}/\Omega_m$.

Schmidt *et al.* [7] derived a model for the mass function enhancement measured in the $f(R)$ N-body simulations. The mass function calculation is based on the Sheth-Tormen prescription using the *linear* power spectrum for the $f(R)$ model, and two limiting cases for the spherical collapse parameters. In one case, we simply assume that the spherical perturbation considered is always larger than the (local) Compton wavelength of the f_R field, so that gravity is GR throughout, and the spherical collapse parameters are unchanged ($\delta_c = 1.673$ and $\Delta_v = 94$ for $\Omega_m = 0.24$). In the second case, we assume that the perturbation is always smaller than the local Compton wavelength, so that forces are enhanced by 4/3. The corresponding modified spherical collapse parameters are $\delta_c = 1.692$ and $\Delta_v = 74$ for $\Omega_m = 0.24$. Figure 1 shows the range of predicted mass function enhancement for these two limiting cases, and the results of the $f(R)$ simulations, for $|f_{R0}| = 10^{-4}$. The mass definition used, $M \equiv M_\Delta$ with $\Delta = 500$ relative to the critical density, is the same as used in the x-ray cluster measurements. In order to obtain conservative upper limits, we choose the modified force prediction for the mass function, which corresponds to the lower bound of the shaded band in Fig. 1.

For a given set of cosmological parameters $(A_s, \Omega_m, h, f_{R0})$, we first calculate the Sheth-Tormen mass functions $dn/d\ln M_v$ for ΛCDM and $f(R)$ using the respective linear power spectra. We then rescale each mass function from the respective virial mass to the common mass definition $M = M_{500}$, using the procedure outlined in [11]. We need to assume a halo profile for this mass rescaling, which we take to be of the Navarro-Frenk-White form with the concentration relation given by [12]. As shown in [7], the profiles of dark matter halos in $f(R)$ within r_v are sufficiently similar to those measured in GR simulations that $f(R)$ effects can be neglected in the mass rescaling. Finally, Δ_v for ΛCDM is obtained from the

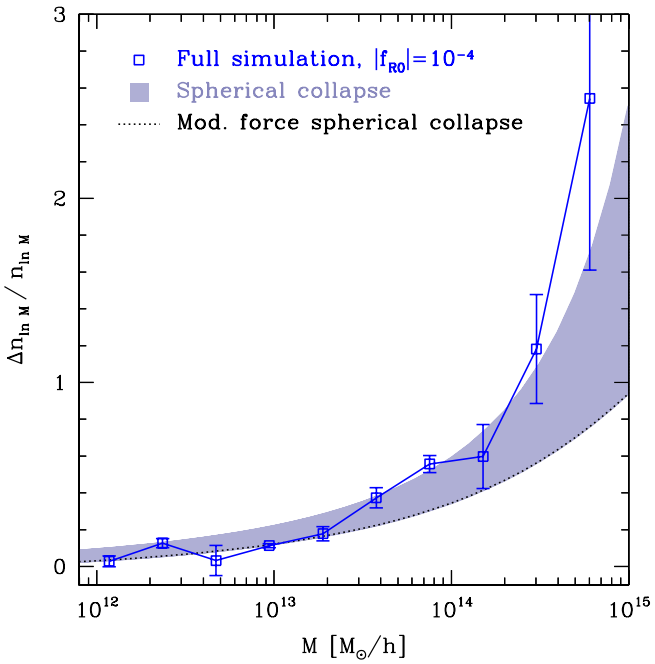

FIG. 1 (color online). Mass function enhancement at $z = 0$ with respect to ΛCDM as a function of $M = M_{500}$, measured in $f(R)$ simulations with $|f_{R0}| = 10^{-4}$. Also shown is the range of spherical collapse predictions from [7]. For the constraints, we conservatively use the lower limit of the shaded band (dashed line).

fitting formula of [13]:

$$\Delta_v^{\rm GR}(\Omega_m) = 178\Omega_m^{0.45}. \quad (11)$$

For the $f(R)$ enhanced forces, we assume the same scaling, fixing the ratio $\Delta_v^{f(R)}/\Delta_v^{\rm GR} = 74/94$. We neglect the small Ω_m dependence of the collapse thresholds within the range of interest, and keep $\delta_c(\Lambda{\rm CDM}) = 1.673$ and $\delta_c(f(R)) = 1.692$ fixed.

III. CLUSTER LIKELIHOOD

In this section we describe the cluster likelihood as a function of cosmological and $f(R)$ parameters. Since we assume a spatially flat cosmology and the expansion history of $f(R)$ models are indistinguishable from ΛCDM, the main cosmological parameters that we have to consider are Ω_m, h, and the primordial normalization A_s at $k = 0.02$ Mpc^{-1}. Other parameters such as the power spectrum tilt do not affect the constraints appreciably [14]. Since the CMB determines $\Omega_m h^2$ to good precision, we are mainly dealing with Ω_m, A_s, and the $f(R)$ parameter f_{R0} for the cluster abundance.

In Sec. III A, we review the likelihood approach taken in Ref. [14]. In Sec. III B, we describe the rescaling of these results for $f(R)$ models.

A. ΛCDM

The cluster sample used in this work is the low-z subsample of 49 clusters described in [14,15]. This is an x-ray flux-limited sample of clusters originally detected in the ROSAT All-Sky Survey at high galactic latitudes and at $z > 0.025$. All of the objects were later observed with Chandra, providing low-scatter proxies for the total mass which can be constructed from the mean x-ray temperature and gas mass (see below). The effective redshift depth of this sample is $z < 0.15$.

Cluster total masses are estimated using the Y_X parameter defined as $Y_X = T_X \times M_{\rm gas}$, where T_X is the average temperature measured from the integral x-ray spectrum, and $M_{\rm gas}$ is the estimated gas mass derived from the analysis of the x-ray surface brightness profile. Y_X is a direct x-ray observable, even though it is hard to backtrack it to raw observables such as the total x-ray luminosity. For a detailed description of the data analysis procedures, see [15].

Based on state-of-the-art cosmological numerical simulations, Y_X is expected to be tightly correlated with the total cluster mass, $M \propto Y_X^{3/5} H(z)^{-2/5}$, with $<10\%$ scatter [16]. Numerical experiments show that the $Y_X - M$ relation is remarkably insensitive to the cluster dynamical state. The power law slope and evolution factor are also insensitive to the details of star formation history and nongravitational heating of the intracluster medium although these processes do change the overall normalization of the relation (e.g., [16,17]). The normalization of the $Y_X - M$ relation was determined observationally [15] using two independent techniques: (1) by the x-ray hydrostatic method using a subsample of dynamically relaxed clusters, and (2) by weak lensing mass measurements. The two methods are in excellent agreement, and this was used to place an upper limit on systematic uncertainties in the cluster mass scale, $\Delta M/M < 9\%$. For our purposes, this agreement also means that the normalization of the $Y_X - M$ relation is tied to the weak lensing measurements, which should provide the true mass in the $f(R)$ theories we consider (Sec. II A).

The cluster component of the likelihood function is computed assuming a purely Poissonian nature of statistical fluctuations[1]:

$$\ln L = \sum_i \ln p(M_i^{\rm est}, z_i) + \sum_i \ln M_i^{\rm est} - \int dz \int dM^{\rm est} p(M^{\rm est}, z), \quad (12)$$

where $M_i^{\rm est}$ and z_i are the estimated mass and redshift of cluster i, $p(M_i^{\rm est}, z_i)$ is the model probability density to observe a cluster with mass $M_i^{\rm est}$ at redshift z_i, and the summation is over the clusters in the sample and integration is over preselected $z_{\rm min} - z_{\rm max}$ and $M_{\rm min} - M_{\rm max}$ intervals. Note that the $\ln M_i^{\rm est}$ term appears because the mass estimates and hence the mass binning required to convert probability densities into probabilities depend on cosmology.

The model probability density, p, is a product of the Tinker *et al.* mass function model [18] for a given set of ΛCDM parameters, cosmological dV/dz function, and the survey selection probability as a function of mass and redshift. The product of these components is convolved with the intrinsic and measurement scatters in the $Y_X - M$ relation. The computation of all these terms is discussed in detail in [15], and the ΛCDM parameter constraints derived from this cluster data set are presented in [14]. We now turn to the computation of the cluster likelihood in the $f(R)$ models.

B. $f(R)$ scaling

A full likelihood analysis of the $f(R)$ cluster constraints would entail a recalculation of the x-ray cluster likelihood grid [14]. Since the modification to the *shape* of the cluster mass function in $f(R)$ is not dramatic across the dynamic range of masses probed by the cluster mass function data (e.g., Figs. 16 and 17 in [15]), we opt for a simpler approach: for each point in parameter space Ω_m, A_s, f_{R0}, we calculate the $f(R)$ mass function enhancement at a pivot mass, $M_{\rm eff} = 3.677 \times 10^{-14} M_\odot/h$. Here we take M to be the true or lensing mass, which is the most conserva-

[1]We ignore a contribution from cosmic variance; the validity of this assumption is justified in [15].

tive assumption. Equating the dynamical mass $M_{\rm dyn} \approx 4M/3$ to the Y_X based mass can only increase the abundance enhancement in the $f(R)$ models. We correspondingly also ignore the additional tension in $f(R)$ implied by the observed agreement between the lensing and Y_X masses.

Then, for this set of parameters, the enhancement is converted to an *effective*, not actual, linear power spectrum normalization, $\sigma_8^{\rm eff}$, assuming a ΛCDM model with the same Ω_m and the mass function prescription of [18]. This approximation assumes that, in the mass range probed by the x-ray clusters, the mass dependence of the mass function enhancement due to $f(R)$ has the same shape as that due to an increased power spectrum normalization. This is only approximately true (see Fig. 2), since the growth is scale dependent in $f(R)$.

In order to benchmark the accuracy of this simplified approach, we recalculated the cluster likelihood for fixed values of Ω_m, h and a range of A_s using the full $f(R)$ mass function, for $|f_{R0}| = 10^{-4}$. We then compared this likelihood with the ΛCDM cluster likelihood calculated for the rescaled normalization, $\sigma_8^{\rm eff}$. The resulting likelihoods are shown as a function of the primordial normalization in Fig. 3. First, clusters clearly prefer a lower primordial

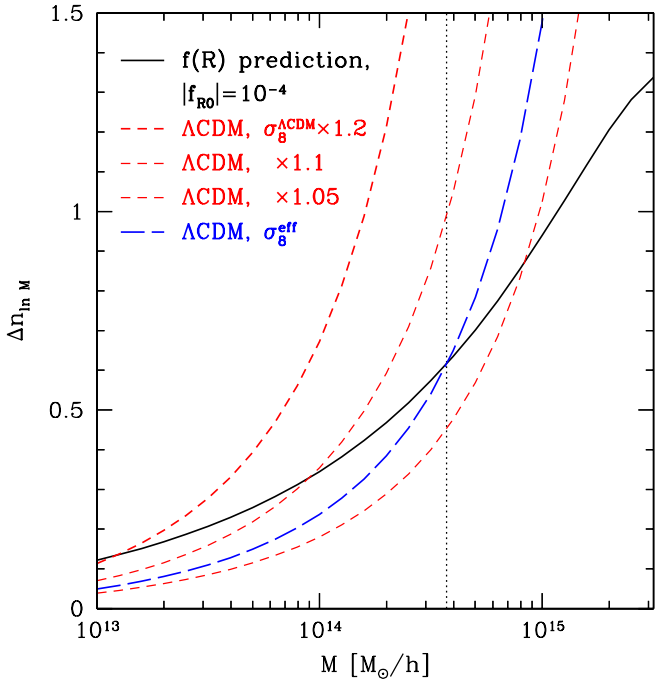

FIG. 2 (color online). Mass function enhancement for $|f_{R0}| = 10^{-4}$ from the spherical collapse model (black, solid line) as in Fig. 1, and the corresponding enhancement when increasing the linear power spectrum normalization in ΛCDM. The vertical line indicates the pivot mass $M_{\rm eff}$ used to calculate the likelihood. The blue long-dashed line shows the enhancement for a rescaled normalization ($\sigma_8^{\rm eff} = \sigma_8 \times 1.066$) that matches the $f(R)$ enhancement at $M_{\rm eff}$.

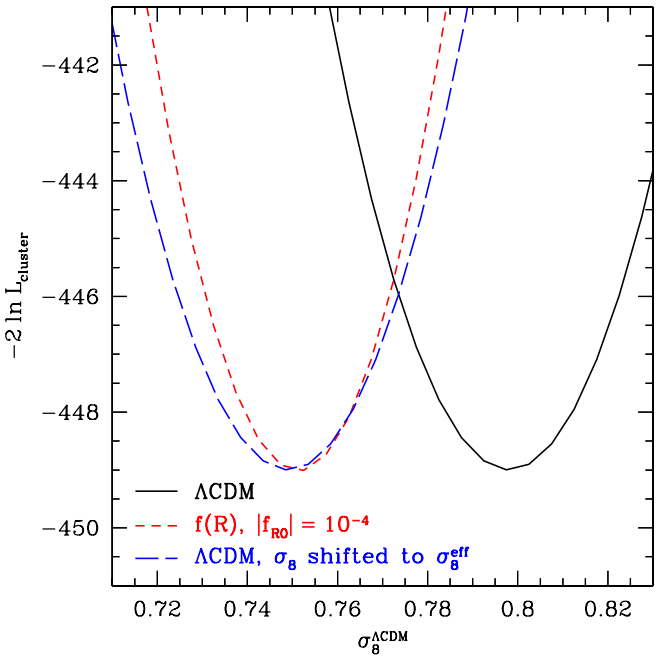

FIG. 3 (color online). Cluster likelihood as a function of primordial normalization (quantified by the linear power spectrum normalization $\sigma_8^{\Lambda CDM}$ a ΛCDM model would give), for fixed values of $\Omega_m = 0.258$, $h = 0.716$, and $|f_{R0}| = 10^{-4}$ in case of the $f(R)$ prediction. The red short-dashed line shows the likelihood calculated using the full $f(R)$ mass function enhancement, while the blue long-dashed line shows the ΛCDM likelihood obtained with the rescaled normalization, $\sigma_8^{\rm eff}$.

normalization in the $f(R)$ model, due to the enhanced growth. The approximate likelihood calculated using the rescaled normalization agrees quite well with the full likelihood. Note that this approach is in any case conservative, as the constraints are weakened (though not significantly) by neglecting the additional information.

While all $f(R)$ mass function enhancements were calculated at $z = 0$, we verified that the evolution of enhancements in the redshift range probed by the cluster sample, $z = 0 - 0.15$, is negligible.

Figure 3 shows that if $\Omega_m \approx 0.26$ and the primordial normalization of the simulations were verified to very high precision by external constraints, and the mass calibration of the cluster sample carried no systematic error, the cluster abundance would be able to rule out the $f(R)$ model with $|f_{R0}| = 10^{-4}$ at around 95% confidence. We next address to what extent these expectations apply to the joint cosmological and cluster data.

IV. COMBINED CONSTRAINTS

The excess cluster abundance predicted in $f(R)$ models can be converted into limits on the field amplitude f_{R0} once data external to the clusters have fixed the background expansion history and primordial normalization of density fluctuations. In Sec. IV A we describe the external data that

we use for these purposes and present combined results in Sec. IV B.

A. External data sets

CMB.—Following Ref. [14], we employ a simplified approach to incorporating CMB constraints from WMAP5 into the cluster analysis. We take three CMB parameters—angular scale of the first acoustic peak, ℓ_A; the so-called shift parameter, R; and the recombination redshift, z_*. The likelihood for the geometric side of the WMAP5 data is computed using the covariance matrix for ℓ_A, R, and z_* provided in [19]. In the ΛCDM expansion history these quantities depend on Ω_m, h, and $\Omega_b h^2$.

Next we add the information contained on the initial amplitude of fluctuations. The WMAP team provides the amplitude of the curvature perturbations at the $k = 0.02\ \mathrm{Mpc}^{-1}$ scale,

$$\hat{A}_s = (2.21 \pm 0.09) \times 10^{-9}. \tag{13}$$

To implement this constraint in terms of $\sigma_8^{\Lambda\mathrm{CDM}}$ and the chosen cosmological parameters we use the fitting formula [20]:

$$A_s^{1/2} \approx \frac{\sigma_8^{\Lambda\mathrm{CDM}}}{1.79 \times 10^4} \left(\frac{\Omega_b h^2}{0.024}\right)^{1/3} \left(\frac{\Omega_m h^2}{0.14}\right)^{-0.563} \times (7.808h)^{(1-n)/2} \left(\frac{h}{0.72}\right)^{-0.693} \frac{0.76}{G_0} \tag{14}$$

(we adjusted numerical coefficients to take into account that the original fit uses the CMB amplitude at $k = 0.05\ \mathrm{Mpc}^{-1}$ while the WMAP5 results are reported for $k = 0.02\ \mathrm{Mpc}^{-1}$). In this equation, G_0 is the growth suppression relative to $\delta \propto (1+z)^{-1}$ due to Λ evaluated today. We then include a χ^2 contribution given by

$$\chi^2_{\mathrm{CMBnorm}} = (A_s \times 10^9 - 2.21)^2 / 0.09^2. \tag{15}$$

The $\chi^2_{\mathrm{CMBnorm}}$ component is computed assuming a fixed $n = 0.95$; the results are completely insensitive to variations of n within the WMAP measurement uncertainties and even to setting $n = 1$. The sum of the geometric and growth component of the CMB χ^2 is marginalized over $\Omega_b h^2$ and h. The end result is a χ^2_{CMB} for the CMB that is a function of Ω_m and $\sigma_8^{\Lambda\mathrm{CDM}}$.

SN.—We use the distance moduli estimated for the type Ia supernovae from the HST sample [21], the SNLS survey [22], and the ESSENCE survey [23], combined with the nearby supernova sample as compiled in Ref. [24]. Calculation of the SN Ia component of the likelihood function for the given cosmological model is standard and can be found in any of the above references. The end result is a χ^2_{SN} that depends on Ω_m only.

H_0.—We use the recent determination of H_0 [25], $H_0 = 74.2 \pm 4.8$ km/s/Mpc, in conjunction with the CMB constraint of $\Omega_m h^2 = 0.133 \pm 0.006$ [26] as a measurement of Ω_m. Marginalizing over the uncertainty in $\Omega_m h^2$ results in the following Gaussian likelihood:

$$\chi^2_{H_0} = \left(\frac{\Omega_m - 0.242}{0.034}\right)^2. \tag{16}$$

BAO.—In a similar way, we use the distance scale given by the baryon acoustic oscillation (BAO) measurements of [27]. We use their Eq. (16), which after marginalizing over $\Omega_m h^2$ yields

$$\chi^2_{\mathrm{BAO}} = \left(\frac{\Omega_m - 0.285}{0.019}\right)^2. \tag{17}$$

The BAO constraint is in fact the most precise one and hence dominates our Ω_m likelihood.

Finally, we combine all the contributions of external data sets

$$\chi^2_{\mathrm{ext}} = \chi^2_{\mathrm{CMB}} + \chi^2_{H_0} + \chi^2_{\mathrm{SN}} + \chi^2_{\mathrm{BAO}}, \tag{18}$$

and add χ^2_{ext} to the cluster likelihood contribution of Eq. (12), $\chi^2_{\mathrm{cl}} \equiv -2 \ln L$.

B. Results

In Fig. 4 (left panel) we show the results of combining the cluster abundance and CMB constraints. The assumption of spatial flatness in combination with the CMB data alone constrains Ω_m and limits the extent of the $f_{R0} - \Omega_m$ degeneracy. Note that the bounds on f_{R0} tighten as Ω_m increases. With only these two data sets the statistical upper limit after marginalizing over Ω_m is $|f_{R0}|/10^{-4} < 8$ at 95% statistical confidence level (C.L.).

Data on SN distances, H_0, and BAO distances tighten the bounds on Ω_m reducing the degeneracy with $|f_{R0}|$. Figure 4 (right panel) shows that the BAO data, in particular, make a strong impact on constraints since they favor high Ω_m. In Fig. 5 we show the $\delta\chi^2$ statistic after marginalization of Ω_m. With all of the data, $|f_{R0}|/10^{-4} < 1.3$ at 95% statistical C.L. Table I summarizes the upper limits on f_{R0} for the different data sets and for different confidence levels.

The main caveat to these statistical constraints is the possibility of systematic shifts in the mass calibration of the cluster sample. In Fig. 6 we show the impact of ±9% shifts in the cluster mass scale on the cluster + CMB constraints. Note that this effect mainly shifts the contours by $\Delta\Omega_m \sim \pm 0.015$. If we assume that cluster masses are *underestimated* ("−9% mass shift," i.e. $M_{X,\mathrm{obs}} = 0.91M$), the abundance at a fixed mass is in fact higher, and hence allows higher f_{R0} values. Conversely, in the case that cluster masses are *overestimated* ("+9% mass shift," i.e. $M_{X,\mathrm{obs}} = 1.09M$), the true abundance at a fixed mass is smaller, hence tightening f_{R0} constraints.

We show the impact of a ±9% mass calibration error on the final joint results in Fig. 7, and in Table I. The net result is that the 95% statistical C.L. carries systematic errors of $+1.7/-0.6 \times 10^{-4}$, which we shall write as $|f_{R0}|/10^{-4} < 1.3^{+1.7}_{-0.6}$.

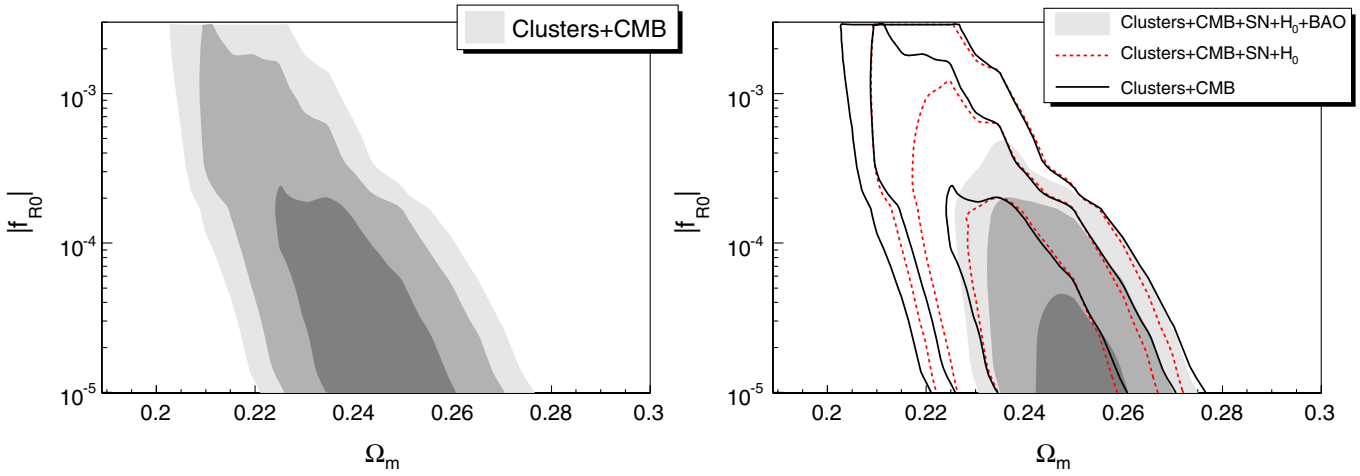

FIG. 4 (color online). Left panel: Likelihood contours from clusters + CMB in the $f_{R0} - \Omega_m$ plane, marginalized over the primordial normalization. Shown are 68.3%, 95.4%, and 99.7% likelihood contours. Right panel: Likelihood contours in the $f_{R0} - \Omega_m$ plane marginalized over the primordial normalization, for clusters + CMB only and when including other geometric measurements.

Note that given $M_{\rm dyn} \approx 4M/3$ in $f(R)$ if there is no screening due to the chameleon mechanism, the x-ray measurements possibly overestimate cluster masses by up to 33%. Hence, we expect that our use of lensing masses in calibrating the enhancement makes our constraint conservative even given the possibility of a 9% underestimate in the x-ray mass measurement.

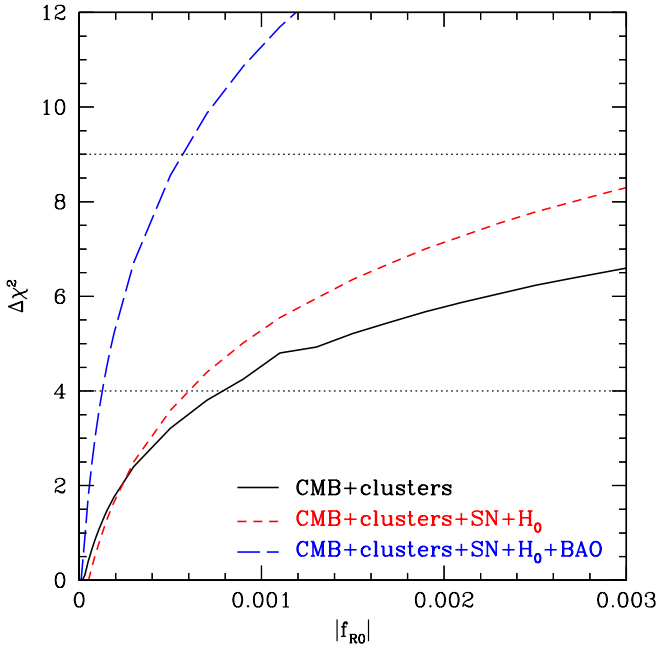

FIG. 5 (color online). Likelihood relative to $f_{R0} = 0$ (ΛCDM) as a function of f_{R0} for CMB + clusters and including other geometric measures. We have marginalized over Ω_m and the primordial normalization. The horizontal lines show the 2σ and 3σ confidence levels. Using all measures combined, $|f_{R0}|/10^{-4} < 1.3$ at 95% confidence level.

Our model of the mass function enhancements (Sec. II C) also represents a lower bound which always underpredicts the enhancement measured in N-body simulations for $10^{-6} < |f_{R0}| < 10^{-3}$ [7]. We have also determined upper limits on $|f_{R0}|$ using the less conservative limiting case presented in [7], which corresponds to using alternate collapse parameters that correspond to the GR values of δ_c and Δ_v. This case is shown as the upper boundary of the shaded band in Fig. 2. While the prediction is still below the simulations, and a better fit, for $|f_{R0}| \gtrsim 10^{-4}$, it overpredicts the enhancements for smaller field values [7]. The last line in Table I shows the resulting limits, which are tighter by a factor of 3–4. We cannot

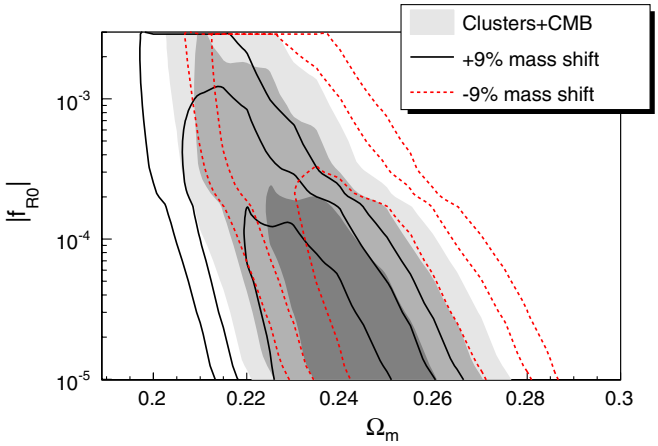

FIG. 6 (color online). Likelihood contours from clusters + CMB in the $f_{R0} - \Omega_m$ plane, marginalized over the primordial normalization as shown in Fig. 4. The solid contours show the results for the standard cluster mass scale, while the black solid (red dashed) lines show the likelihood in case cluster masses are overestimated (underestimated) by 9%.

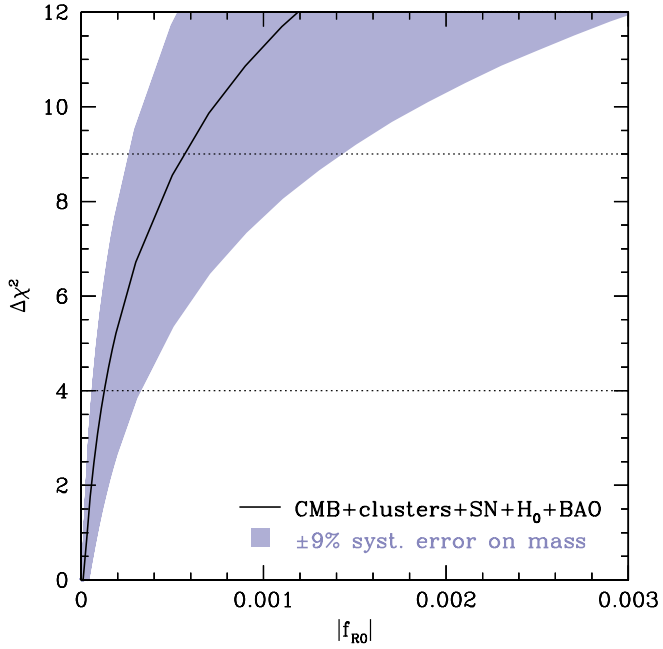

FIG. 7 (color online). Likelihood as a function of f_{R0} as in Fig. 5 for CMB + clusters and all geometric measures. The shaded band shows the weakening/strengthening of the constraints when varying the absolute mass scale by ±9%, corresponding to the estimated systematic uncertainty. In the weakened case (masses underestimated), the constraint degrades to $|f_{R0}|/10^{-4} < 3.0$ at 95% confidence level.

TABLE I. Upper limits on f_{R0} in units of 10^{-4}.

Confidence level (C.L.)	68.3%	95.4%	99.7%
Clusters + CMB	1.0	7.9	>31
Clusters + CMB + SN + H_0	1.0	5.4	>31
Clusters+CMB+SN+H_0+BAO	**0.3**	**1.3**	**6.3**
with +9% mass shift	0.2	0.7	3.1
with −9% mass shift	0.7	3.0	14.7
with alternate collapse parameters	0.09	0.4	1.8

guarantee that this model does not overpredict the enhancement in some region of the parameter space involved, but the corresponding tightening of the constraints again indicates that our quoted limit should be viewed as conservative.

V. DISCUSSION

We have provided the first, simulation calibrated, cluster abundance constraints on a modified gravity model, specifically $f(R)$ gravity. Enhanced forces below the Compton wavelength of the scalar field lead to corresponding enhancements in the cluster abundance, making the latter a sensitive probe of gravity on cosmological scales.

Combined with constraints on the primordial amplitude of fluctuations from the CMB, and geometric constraints from CMB, supernovae, H_0, and BAO, the cluster abundance provides the most stringent constraint on these enhancements to date. In terms of the field amplitude today, the constraint is $|f_{R0}|/10^{-4} < 1.3^{+1.7}_{-0.6}$, where the range reflects a $\mp 9\%$ mass calibration error, an improvement over previous constraints by 4 orders of magnitude. This corresponds to an upper limit on the range of the gravitational force modifications of $\lambda_C < 38^{+19}_{-10}$ Mpc in this $f(R)$ model.

Our constraint should be viewed as conservative even given the 9% mass calibration error. We have ignored an overestimate of dynamically based x-ray masses over true or lensing masses, which could be up to a 33% shift that would further enhance the abundance and strengthen the constraint. In addition, we have not considered the possibility of constraining $f(R)$ force modifications from the comparison of cluster lensing and dynamical masses.

Furthermore, our model of the mass function enhancements represents a conservative lower bound which always underpredicts the enhancement measured in N-body simulations. We found that the constraints tighten significantly if we use a less conservative model but a robust implementation would require more accurate mass function calibration across the parameter space.

On the observational side, current constraints are limited mainly by systematics in the mass calibration and secondarily by the small number of local clusters. Relaxing the assumption of a flat universe is not expected to degrade the upper limits appreciably. This is because our constraints only depend strongly on the allowed range in Ω_m and marginalizing over curvature changes this range negligibly once BAO are combined with SN and/or the CMB [27].

In the future, the abundance of massive clusters could ultimately provide another order of magnitude improvement in the field amplitude to $|f_{R0}| \sim 10^{-5}$, rivaling solar system tests of gravity but in a very different, low curvature regime [5]. Below field values of $\sim 10^{-5}$, the chameleon mechanism suppresses the enhancement at the high mass end [7]. In this regime, further improvements are potentially available if the abundance of galaxy groups can provide constraints on the halo abundance at intermediate masses.

While we have considered a specific functional form of $f(R)$ here [5], different functional forms have been proposed in the literature, see e.g. [28–30]. These models differ primarily in the evolution with redshift of the Compton wavelength of the f_R field. Hence, we expect our results to be generic once the field amplitude and range are rescaled to some effective redshift which matches the impact on the linear growth today on a scale relevant for clusters. For example in models where the curvature dependence is steeper, the field amplitude today is allowed to be larger since its current value has little impact on the growth of structure. In these models solar system tests become even more powerful relative to cosmological tests.

More generally, the abundance of galaxy clusters promises to be a good probe of other modified gravity scenarios as well, such as Dvali-Gabadadze-Porrati and other brane-world models once their mass functions are calibrated by cosmological simulations [31,32].

ACKNOWLEDGMENTS

We thank the Aspen Center for Physics where part of this work was completed. F. S. and W. H. were supported by the Kavli Institute for Cosmological Physics (KICP) at the University of Chicago through Grants NSF No. PHY-0114422 and NSF No. PHY-0551142 and an endowment from the Kavli Foundation and its founder Fred Kavli. W. H. was additionally supported by the U.S. Department of Energy Contract No. DE-FG02-90ER-40560 and the David and Lucile Packard Foundation. A. V. was supported by NASA Grants and Contracts No. NAG5-9217, No. GO5-6120A, No. GO6-7119X, and No. NAS8-39073. Computational resources for the cosmological simulations were provided by the KICP-Fermilab computer cluster.

[1] S. M. Carroll, V. Duvvuri, M. Trodden, and M. S. Turner, Phys. Rev. D **70**, 043528 (2004).
[2] S. Nojiri and S. D. Odintsov, Phys. Rev. D **68**, 123512 (2003).
[3] S. Capozziello, S. Carloni, and A. Troisi, Recent Res. Dev. Astron. Astrophys. **1**, 625 (2003).
[4] J. Khoury and A. Weltman, Phys. Rev. D **69**, 044026 (2004).
[5] W. Hu and I. Sawicki, Phys. Rev. D **76**, 064004 (2007).
[6] Y.-S. Song, H. Peiris, and W. Hu, Phys. Rev. D **76**, 063517 (2007).
[7] F. Schmidt, M. Lima, H. Oyaizu, and W. Hu, Phys. Rev. D **79**, 083518 (2009).
[8] J. D. Bekenstein and R. H. Sanders, Astrophys. J. **429**, 480 (1994).
[9] H. Oyaizu, Phys. Rev. D **78**, 123523 (2008).
[10] H. Oyaizu, M. Lima, and W. Hu, Phys. Rev. D **78**, 123524 (2008).
[11] W. Hu and A. V. Kravtsov, Astrophys. J. **584**, 702 (2003).
[12] J. S. Bullock *et al.*, Mon. Not. R. Astron. Soc. **321**, 559 (2001).
[13] V. R. Eke, J. F. Navarro, and C. S. Frenk, Astrophys. J. **503**, 569 (1998).
[14] A. Vikhlinin *et al.*, Astrophys. J. **692**, 1060 (2009).
[15] A. Vikhlinin *et al.*, Astrophys. J. **692**, 1033 (2009).
[16] A. V. Kravtsov, A. Vikhlinin, and D. Nagai, Astrophys. J. **650**, 128 (2006).
[17] P. Bode, J. P. Ostriker, and A. Vikhlinin, Astrophys. J. **700**, 989 (2009).
[18] J. L. Tinker *et al.*, arXiv:0803.2706.
[19] E. Komatsu *et al.*, arXiv:0803.0547.
[20] W. Hu and B. Jain, Phys. Rev. D **70**, 043009 (2004).
[21] A. G. Riess *et al.*, Astrophys. J. **659**, 98 (2007).
[22] P. Astier *et al.* (SNLS Collaboration), Astron. Astrophys. **447**, 31 (2006).
[23] W. M. Wood-Vasey *et al.* (ESSENCE Collaboration), Astrophys. J. **666**, 694 (2007).
[24] T. M. Davis *et al.*, Astrophys. J. **666**, 716 (2007).
[25] A. G. Riess *et al.*, Astrophys. J. **699**, 539 (2009).
[26] E. Komatsu *et al.*, Astrophys. J. Suppl. Ser. **180**, 330 (2009).
[27] W. J. Percival *et al.*, arXiv:0907.1660.
[28] S. Appleby and R. Battye, Phys. Lett. B **654**, 7 (2007).
[29] A. A. Starobinsky, Sov. J. Exp. Theor. Phys. Lett. **86**, 157 (2007).
[30] S. Nojiri and S. D. Odintsov, Phys. Lett. B **657**, 238 (2007).
[31] J. Khoury and M. Wyman, Phys. Rev. D **80**, 064023 (2009).
[32] F. Schmidt, Phys. Rev. D **80**, 043001 (2009).